Published in final edited form as:
Cell Stem Cell. 2014 November 6; 15(5): 559–573. doi:10.1016/j.stem.2014.10.006.

Human PSC-derived maturing GABAergic interneurons ameliorate seizures and abnormal behavior in epileptic mice

Miles Cunningham[c,#], **Jun-Hyeong Cho**[d,f,#], **Amanda Leung**[a,b], **George Savvidis**[a,b], **Sandra Ahn**[a,b], **Minho Moon**[a,b], **Paula KJ Lee**[a,b], **Jason J. Han**[e], **Nima Azimi**[c], **Kwang-Soo Kim**[a,b], **Vadim Y. Bolshakov**[d], and **Sangmi Chung**[a,b,*]

[a]Molecular Neurobiology Laboratory, Department of Psychiatry and Program in Neuroscience, McLean Hospital/Harvard Medical School, Belmont, MA 02478, USA

[b]Harvard Stem Cell Institute, McLean Hospital/Harvard Medical School, Belmont, MA 02478, USA

[c]Laboratory for Neural Reconstruction, Department of Psychiatry, McLean Hospital/Harvard Medical School, Belmont, MA 02478, USA

[d]Cellular Neurobiology Laboratory, Department of Psychiatry, McLean Hospital/Harvard Medical School, Belmont, MA 02478, USA

[e]MRC Electron and Light Microscopy Core Facility, McLean Hospital/Harvard Medical School, Belmont, MA 02478, USA

Summary

Seizure disorders debilitate more than 65,000,000 people worldwide, with temporal lobe epilepsy (TLE) being the most common form. Previous studies have shown that transplantation of GABA-releasing cells results in suppression of seizures in epileptic mice. Derivation of interneurons from human PSC has been reported, pointing to clinical translation of quality-controlled human cell sources that can enhance inhibitory drive and restore host circuitry. In this study, we demonstrate that human PSC-derived maturing GABAergic interneurons (mGIN) migrate extensively and integrate into dysfunctional circuitry of the epileptic mouse brain. Using optogenetic approaches, we find that grafted mGINs generate inhibitory postsynaptic responses in host hippocampal neurons. Importantly, even before acquiring full electrophysiological maturation, grafted neurons were capable of suppressing seizures and ameliorating behavioral abnormalities such as cognitive

[*]*Corresponding* author; Sangmi Chung, Ph.D., McLean Hospital/Harvard Medical School, 115 Mill Street, Belmont, MA 02178, Tel: 617-855-3478; Fax: 617-855-2020, schung@mclean.harvard.edu.
[#]denotes equal contributions.
[f]Present Address: Department of Cell Biology and Neuroscience, University of California, Riverside, Riverside, CA 92521, USA

SUPPLEMENTAL INFORMATION

Supplemental Information includes seven figures, and two tables and Supplemental Experimental Procedures and can be found with this article online at http://dx.doi.org/.

Author Contributions

MC, JC, MM and SC designed the experiments. MC, JC, AL, SA, GS, MM, PL, JH, NA and SC conducted experiments, collected data and analyzed data. MC, JC, MM, VB and SC wrote manuscript.

deficits, aggressiveness and hyperactivity. These results provide support for the potential of human PSC-derived mGIN for restorative cell therapy for epilepsy.

Introduction

Epileptic seizures are characterized by unpredictable abnormal electrical discharge, loss of consciousness and convulsions, and they are experienced by one in 26 individuals at some point in their lifetime (Jensen, 2014). One of the most common forms of seizures is temporal lobe epilepsy (TLE), characterized by epileptic abnormalities in the hippocampus, parahippocampal gyrus and amygdala (Engel, 2001). About one third of patients with TLE exhibit intractable seizures that cannot be controlled by anti-epileptic drugs (AEDs) (Engel, 2002), and surgical resection of the seizure focus may be necessary (Christoph, 2008). Patients who are not candidates for surgery must live with ongoing seizures – in many cases, multiple events in a single day. Although AEDs can reduce or eliminate seizures for the more fortunate patients, these medicines are associated with diverse and troublesome side effects, including weight gain, metabolic acidosis, hepatotoxicity, movement disorders, and mental status changes (Cramer et al., 2010; Walia et al., 2004). More effective, permanent therapeutic solutions are desperately needed for many of these patients with limited treatment options.

A key pathological feature of human TLE is synaptic reorganization, including neuronal loss and gliosis in CA1 and hilus, granule cell dispersion, and mossy fiber sprouting in the dentate gyrus (Wieser, 2004). Examination of excised epileptic tissue from TLE patients has revealed a loss of interneurons releasing inhibitory neurotransmitter GABA (de Lanerolle et al., 1989; Marco et al., 1996; Spreafico et al., 1998). It is believed that a decrease in GABA-mediated inhibition is a critical contributing factor in epilepsy. Indeed, decreased inhibition has repeatedly been demonstrated in TLE animal models (Cossart et al., 2001; Hirsch et al., 1999; Kobayashi and Buckmaster, 2003). Therefore, one possible therapeutic approach is to increase GABA-mediated inhibition to suppress hyperexcitable neurons during seizure initiation. Early work exploring the potential for inhibitory neural grafts in controlling epileptic activity has shown promise and has inspired further studies (Fine et al., 1990; Lindvall and Bjorklund, 1992; Loscher et al., 1998). More recent experiments have shown that mouse GABAergic interneuron precursors engrafted into the TLE mouse brain decreased seizure activity (Baraban et al., 2009; Hattiangady et al., 2008; Hunt et al., 2013; Maisano et al., 2012; Southwell et al., 2014).

However, to transform such proof-of-principle studies into viable therapeutic approaches for human TLE patients, it is critical to develop optimal human cell sources that can integrate into host circuitry, increase GABA-mediated inhibitory tone, and thereby reduce seizure activity in the epileptic brain. Human PSC technologies, including induced pluripotent stem cells (iPSC), have the potential to provide an unlimited and ethically unimpeded source of therapeutic cells (Chen et al., 2014; Mallon et al., 2013; Yu et al., 2013) including human interneurons. Nevertheless, efficient translation of hPSC-derived interneurons could be hampered by their well-known, protracted maturation (Le Magueresse and Monyer, 2013; Nicholas et al., 2013). For example, parvalbumin^{+} neurons acquire fast-spiking property

only after postnatal maturation into early adolescence in mice (Doischer et al., 2008; Okaty et al., 2009).

Using highly efficient methods for generating medial ganglionic eminence (MGE) cells, precursors of mGIN, from human PSCs (Kim et al., 2014), we transplanted a homogeneous population of human MGE cells into pilocarpine-induced TLE mice, a well-characterized model of human TLE (Curia et al., 2008). Then, we extensively characterized the biology of human PSC-derived mGIN within the epileptic brain. mGIN actively migrate, spreading throughout the entire host hippocampus. Using optogenetic approaches and ultrastructural studies, we demonstrated that grafted mGIN integrate into the dysfunctional host circuitry, receive excitatory inputs and, in turn, induce inhibitory responses in host neurons by releasing GABA. This ultimately resulted in the reversal of behavioral abnormalities in TLE mice, including spontaneous seizures as well as comorbid cognitive impairment, hyperactivity, and aggressiveness. These findings have compelling implications for the previously undescribed utility of human PSC-derived mGIN to address a desperate need for new therapies to treat seizure disorders.

Results

Human mGIN extensively migrate within the epileptic brain

Human MGE cells were generated by in vitro differentiation of H7 human embryonic stem cells according to our optimized procedure (Kim et al., 2014), and purified by FACS using anti-ENCAM antibody prior to transplantation (Fig. 1a). Most of the FACS-sorted cells expressed the MGE markers Nkx2.1 and Olig2, as well as the early neural marker nestin, but no cells were positive for the pluripotent stem cell marker SSEA4 (Fig. S1). We generated a mouse model for temporal lobe epilepsy (TLE) by injecting Nod-Scid mice with 400mg/kg doses of pilocarpine. Animals demonstrating Racine stage 3–5 seizure activity upon induction with pilocarpine were further screened for occurrence of spontaneous recurrent seizures (SRS) over 7 days using continuous video monitoring starting 10 days after pilocarpine injection. Mice having at least one SRS during this 7-day screening period were used for further experiments and were denoted as “TLE mice” in this study. Human MGE cells were disseminated throughout most of the hippocampus by depositing volumes of cell suspension within the rostral and caudal hippocampus bilaterally using 4 separate targets on each side as reported previously (Hunt et al., 2013) (Fig. 1a). Histological analysis showed that 2 weeks post-transplantation (PT), cells were primarily clustered near the injection site (59,027±18,724 total human nucleus$^+$ cells per mouse, n=3; Fig. 1b–c). At 4 months PT, however, transplanted mGIN had extensively migrated, becoming well integrated within the host hippocampus (74,913±15,417 total human nucleus$^+$ cells per mouse, n=8; Fig. 1d–j, Fig. S2 and Fig. S4), without significant difference in the total surviving cell numbers compared to 2 weeks PT (p=0.58). Stereological analysis demonstrated migration of transplanted human mGIN greater than 1.6 mm from the site of injection (Fig. 1k). At 2 weeks PT, most cells expressed GABA, Sox6 as well as Nkx2.1 (Fig. 2a–c), with a minority of cells expressing the more mature neuronal marker NeuN (Fig. 2e). However, at 4 months PT, the majority of cells expressed NeuN as well as GABA and Sox6 (Fig. 2g–h, j and r). The expression of precursor marker Nkx2.1 was significantly diminished at 4 months PT

compared to 2 weeks PT (Fig. 2i and w), whereas the mature interneuron marker Lhx6 was significantly increased at 4 months PT compared to 2 weeks PT (Fig.2 d, k and w). In addition, proliferating cell marker Ki67 was significantly decreased after 4 month PT compared to 2 weeks PT (Fig. 2f, l and w). Further, at 4 months PT, some GABAergic interneurons were found to express somatostatin, parvalbumin, calretinin, neuropeptide Y and calbindin (Fig. 2m–q, x and Fig. S5af). As seen during in vivo embryonic development, interneuron maturation was not synchronous and cells with simple bipolar morphology and cells with more complex neurites coexist at this time point (Fig S5 g–l). Transplanted cells generated very small numbers of astrocytes ($GFAP^+$; Fig. 2u and x) or oligodendrocyte lineage cells ($Olig2^+$; Fig. 2v and x).

Functional integration of human mGIN into the epileptic brain

Electrophysiological and morphological analyses were used to determine whether transplanted human MGE cells develop into functional GABAergic neurons and integrate into host neural circuitry. Human MGE cells, transduced with lentivirus to stably express channelrhodopsin-2 (ChR2) (H134R)-GFP fusion under a synapsin promoter, were transplanted into the hippocampus of TLE mice. Two to five months after transplantation, grafted human MGE-derived cells were identified with green fluorescence in acute brain slices containing the hippocampus (GFP^+ cells, Fig. 3a). All 31 GFP^+ cells displayed typical ChR2-mediated currents induced by blue light illumination (Fig. 3b), indicating that recorded GFP^+ cells were indeed human MGE-derived cells expressing ChR2. Consistently, short pulses of blue light illumination evoked action potential (AP) firings in most GFP^+ cells (Fig. 3c), suggesting that grafted GFP^+ cells can be activated by photostimulation in brain slice preparations. Passive membrane properties of GFP^+ human mGIN, including resting membrane potential (RMP) and membrane resistance (R_m), were similar to those reported previously (Nicholas et al., 2013) (Fig. 3d). Unlike the previous report, however, we did not observe an increasing trend of the membrane capacitance (C_m) of the grafted cells (Fig. 3d). This discrepancy may be due to the different experimental conditions that human MGE cells were transplanted into the brain in our study whereas they were grown in culture in the previous report. Thus, our findings reflect the membrane properties of human MGE cells under more physiological conditions. Compared to host hippocampal interneurons in adult mice, RMP was significantly depolarized in grafted mGIN (Fig. 3d, $p < 0.001$), suggesting that grafted cells were not fully mature at this time point. However, there was no significant difference in R_m and C_m between human mGIN vs. host interneurons. When voltage pulses were applied, grafted human mGIN showed rapidly desensitizing inward currents activated at membrane potential > –40 mV (Fig. 3e), indicating the expression of voltage-gated Na^+ channels. In current-clamp mode, 45% of human mGIN displayed spontaneous AP firings at resting membrane potential at 2.0 ± 0.2 Hz (Fig. 3f and g), suggesting that some of the grafted mGIN generate tonic firings.

Furthermore, the injection of depolarizing currents induced AP firings in all human mGIN examined (Fig. 4a and b). As for passive membrane properties, grafted mGIN displayed less mature biophysical properties of AP firings compared to the host interneurons in terms of after-hyperpolarization and AP width (Fig. 4b), consistent with their well-known protracted maturation (Nicholas et al., 2013), whereas there was no significant difference in AP

threshold. When grouped based on AP firing, most human mGIN displayed repetitive (type A, 52%) or single AP firing (type B, 32%) whereas delayed (13%) or burst firing pattern (3%) was also observed in a small proportion of transplanted cells (Fig. 4c). Furthermore, while more frequent AP firings were induced by small current injections (< 50 pA) in repetitive-firing type A cells, type B cells generated only 1–3 AP firings induced by much larger current injections (> 50 pA, Fig. 4e). As expected, R_m was significantly larger in type A cells than in type B cells (Fig. 4e), accounting for different firing patterns of these cells.

After recording, we collected the intracellular contents of the recorded cells and performed single-cell RT-PCR to examine the RNA profile of transplanted human mGIN (Fig. 4f). Most grafted cells expressed glutamate decarboxylase (GAD) and Sox6 while some grafted cells also expressed other GABAergic neuronal markers including parvalbumin, calreticulin, somatostatin, vasoactive intestinal peptide, and neuropeptide Y (Fig. 4g). We also performed morphological analysis with biocytin-labeled human mGIN and found characteristic neuronal morphologies with various patterns of neuronal processes (Fig. S6). These results therefore demonstrate that transplanted human MGE cells develop into mGIN with diverse electrophysiological, biochemical and morphological properties in the epileptic hippocampus.

We then investigated whether grafted human mGIN possessed functional postsynaptic mechanisms allowing synaptic transmission from host neurons. Using confocal microscopic imaging, we observed postsynaptic dendritic spines in biocytin-labeled grafted cells, suggesting that they may receive excitatory synaptic inputs (Fig. 5a and b). Consistently, in acute hippocampal slices, two thirds of 21 GFP^+ mGIN showed spontaneous postsynaptic currents at –85 mV in voltage-clamp mode at a frequency > 0.1 Hz (Fig. 5c and e). Moreover, these currents were inhibited completely by NBQX, an AMPA/kainite-type glutamate receptor antagonist (Fig. 5d), indicating that they were mediated by excitatory neurotransmitter glutamate. There were no significant differences in biophysical properties of spontaneous postsynaptic activities between grafted human mGIN and host hippocampal interneurons (Fig. 5f–i). These results suggest that most human mGIN transplanted into the hippocampus, have functional postsynaptic machinery, receiving excitatory synaptic inputs from host glutamatergic neurons. Immunocytochemistry analysis also showed that many postsynaptic $PSD95^+$ puncta on GFP^+ grafted cells were juxtaposed with presynaptic synaptophysin puncta (Fig. 5j; 2.18 ± 0.56 $PSD95^+$ puncta/10 μm GFP^+ dendrite, n=22 dendrite segments), suggesting the formation of host glutamatergic synapses onto transplanted human mGIN. Further confirmation of functional synapse formation between host and transplanted neurons was obtained from ultrastructural analysis by Transmission Electron Microscopy (TEM). Examination of hippocampal areas in brain slices immunostained with diaminobenzidine (DAB) for human cytoplasm (human $cytoplasm^+$) showed excitatory synaptic connections onto grafted mGIN (Fig. 5k–l). These combined electrophysiological and ultrastructural data demonstrate functional synaptic integration of grafted mGIN into host parenchyma.

Activation of human mGIN induces GABA-mediated inhibitory postsynaptic responses in host hippocampal neurons

We next investigated whether grafted human mGIN also have functional presynaptic machinery to release GABA and induce inhibitory postsynaptic responses in host hippocampal neurons (Fig. 6a). To this end, we used optogenetic approaches to selectively stimulate ChR2-expressing transplanted cells in hippocampal slices (Fig. 6b). Blue light illumination induced ChR2-mediated inward current and AP firings in GFP^+ grafted cells (Fig. 3c), whereas the same photostimulation did not induce such currents in any GFP^- cells tested (Fig. 6b), suggesting that grafted cells can be selectively activated in acute brain slices with this approach. Under these conditions, short pulses of photostimulation, activating ChR2-expressing grafted cells, induced postsynaptic responses in 44% of total 27 GFP^- cells (Fig. 6c and d). The recorded postsynaptic currents showed a short synaptic delay, indicating monosynaptic origin (Cho et al., 2013). Furthermore, these synaptic responses were inhibited completely by bicuculline, a $GABA_A$ receptor antagonist (Fig. 6c and d), suggesting that they were mediated by inhibitory neurotransmitter GABA. The current-voltage relationship revealed the reversal potential of these currents at –70 ± 3 mV (Fig. 6e), consistent with the estimated reversal potential of chloride ion (–65 mV under our experimental conditions). In some GFP^- cells, photostimulation induced probabilistic quantal responses (Fig. 6f and g), confirming their synaptic nature. Moreover, train photostimulation at 1 Hz induced postsynaptic responses without significant reduction in peak amplitude (Fig. 6h and i), suggesting that the repetitive activation of grafted mGIN can consistently induce GABAergic responses in GFP^- cells. Considering that grafted cells constitutes 30.7 ± 4.7% of total cells at the graft core, where the density of GFP^+ cells is highest, the majority of the recorded GFP^- cells would be host hippocampal neurons. Thus, our results suggest that the activation of transplanted human MGE-derived cells can generate inhibitory postsynaptic responses in host hippocampal neurons. Imaging studies provided further evidence for the formation of inhibitory synaptic connections onto host neurons by transplanted human mGIN. Fluorescence microscopy showed that many of the presynaptic $VGAT^+$ puncta on GFP^+ mGIN were juxtaposed with postsynaptic $Gephyrin^+$ puncta (Fig. 6j). TEM ultrastructural studies also identified symmetric synaptic contacts between presynaptic grafted cells and postsynaptic host neurons (Fig. 6k–l). These combined results suggest that grafted human mGIN have presynaptic machinery to release GABA and inhibit host hippocampal neurons as well as postsynaptic machinery to receive excitatory inputs from host neurons.

Human mGIN reduce seizure activity in epileptic mice and ameliorate behavioral abnormalities

Our electrophysiological findings suggest that transplanted human mGIN integrate into host hippocampal circuitry and may be sufficient to exert anti-epileptic effects by releasing inhibitory neurotransmitter GABA and increasing inhibitory synaptic responses in host hippocampal neurons. Therefore, we next investigated the therapeutic potential of transplanted human mGIN for preventing seizures in our TLE mouse model. Seizure activity of engrafted TLE mice was analyzed 3 months after transplantation by continuous EEG-video monitoring. Vehicle-injected control TLE mice with sham surgery (n=11) showed seizure EEG activity with high-frequency and high-voltage synchronized polyspikes (Fig.

4a), having a seizure event frequency of 1.92 ± 0.45 seizures/day. mGIN-grafted TLE mice (n=9), however, showed significantly reduced seizure event frequency (0.13 ± 0.07 seizure/day); in five animals in this group, seizure activity was eliminated entirely (Fig. 4a). Seizure EEG activity was confirmed by simultaneous video recording, which showed clonus and rearing and falling of the mice (Racine stage 3–5; Video. S1). Naïve Nod-Scid mice without pilocarpine injection did not show any seizure EEG activity during the monitoring (n=6). The duration of seizures was not significantly different between control TLE mice and mGIN-grafted TLE mice (39 ± 2.7sec vs. 42.8 ± 8.7 sec, n = 4–10, p = 0.61). These results indicate that transplantation of human mGIN suppresses seizure activity in the TLE mouse model.

Because epilepsy patients frequently suffer from comorbid cognitive impairment and psychiatric symptoms (Brooks-Kayal et al., 2013), we next analyzed the effect of human mGIN transplantation on other behavioral abnormalities of TLE mice. Previous studies have shown that these animals, similar to TLE patients, show cognitive deficits (Groticke et al., 2007), which could be reversed by engrafting mouse fetal MGE cells (Hunt et al., 2013). Therefore, we tested whether transplanted mGIN can improve cognitive function of TLE mice in a similar manner. In a Y maze test, control TLE mice (n=10) showed significant deficits in short-term working memory compared to naïve mice (n=9). This deficit was dramatically abolished after mGIN transplantation (n=8), whereas there was no significant difference in total arm entry among test groups (p=0.49, Fig. 4b). In novel object recognition test, an independent measure of learning and memory, control TLE mice (n=11) showed significantly decreased time exploring the novel object compared to the naïve mice (n=12), whereas this deficit was reversed after mGIN transplantation (n=8; Fig. 4c). The frequency of novel object exploration showed a similar trend as the duration of novel object exploration, but did not reach statistical significance (p=0.19). These data suggest that transplantation of human mGIN can reduce cognitive deficits in rodent model of TLE.

In addition to cognitive deficits, hyperactivity and aggressiveness have been reported in the pilocarpine-induced rodent model of TLE (Muller et al., 2009; Rice et al., 1998). Consistently, control TLE mice (n = 11) displayed significantly higher locomotor activity compared to the naïve mice (n=14) as measured using a photobeam activity system. However, animals engrafted with human mGIN displayed a significant attenuation of this abnormality (n=8; Fig. 4d). Moreover, hypervigilance and aggressiveness normally observed in control TLE mice (n=11) were completely reversed to levels of naïve mice (n=15) after transplantation of human mGIN (n=10; Fig. 4e and Video S2). In sum, these results suggest that transplantation of human mGIN suppresses seizure activity in epileptic mice and ameliorates other behavioral abnormalities.

Discussion

While fetal MGE cell transplantation has demonstrated proof-of-principle for cell-based therapy of epilepsy (Hattiangady et al., 2008; Hunt et al., 2013), clinical application is limited by the lack of standardized and reliable cell sources as well as ethical controversies associated with using fetal cells. Human PSC technology offers the potential to provide cell sources that are well-characterized, quality-controlled, and virtually unlimited in supply, as

long as efficacious progenies can be proficiently derived. We have utilized optimized differentiation of human PSCs into MGE cells (Kim et al., 2014), and report here previously unknown functional efficacy of mGIN to reduce epileptic activity and comorbid behavioral abnormalities in the epileptic brain even before they attain full maturity. Considering full electrophysiological maturation of human GABAergic interneurons could take years (Le Magueresse and Monyer, 2013; Nicholas et al., 2013), our findings using human mGIN provide a major step towards developing an efficient and novel cell-based therapy for treating intractable epilepsy.

We have demonstrated that PSC-derived human mGIN migrate extensively within the epileptic hippocampus, integrate into host circuitry and reduce seizure activity and other behavioral abnormalities. The primary mechanisms of the functional effects of grafted mGIN are suggested by our electrophysiological studies. Although they are not fully mature, approximately half of transplanted human MGE cells fire spontaneous action potentials (AP) at ~2 Hz, indicating that they are tonically active even without extrinsic synaptic inputs. Moreover, transplanted human mGIN fully integrate into the hippocampal circuitry, receiving excitatory synaptic inputs from host glutamatergic neurons, and are therefore activated by host signals. In turn, our optogenetic studies revealed that grafted human mGIN release inhibitory neurotransmitter GABA in an activity-dependent manner. Therefore, the activation of transplanted mGIN, either by spontaneous activity or by excitatory synaptic drive, causes an increase of inhibitory synaptic responses in host hippocampal neurons, shifting excitation/inhibition balance toward inhibition and suppressing exaggerated neural activity in the epileptic brain. Consistent with previous work (Hunt et al., 2013), we did not observe significant changes in mossy fiber sprouting by human MGE transplantation compared to control TLE mice (Fig. S7), suggesting that regulation of inhibitory balance alone by grafted cells may be sufficient to exert the anti-epileptic effects observed in this study.

Cell therapy for epilepsy offers a number of advantages over conventional therapies. Distinct cell types can be precisely engrafted into brain substructures (Bjarkam et al., 2010), averting the acute and long-term systemic adverse effects seen with AEDs. Further, neural grafts, with their ability to integrate within the host circuitry, would circumvent the need for daily dosing and sluggish titration required with AED administration. A self-regulating therapeutic system of mGIN grafts would eliminate the need of carrying devices to monitor and control seizures. Temporal lobectomy has been used as a last-resort intervention for intractable epilepsy, but is associated with surgical morbidity and permanent dysfunction. High-precision stereotactic engraftment of stem cells, however, is less invasive and leaves functional neural tissue undisturbed.

Here we have demonstrated the biology and utility of human PSC-derived mGIN to ameliorate the symptoms of a prevalent and debilitating neuropsychiatric disease. While the efficacy of mouse fetal interneurons to ameliorate seizure activity has been demonstrated previously (Baraban et al., 2009; Hattiangady et al., 2008; Hunt et al., 2013; Maisano et al., 2012; Southwell et al., 2014), the current investigation is the first to demonstrate the therapeutic efficacy of human PSC-derived interneurons to treat epilepsy, and it represents the potential for a reliable and ethically unimpeded cell source for this purposes. Before

transition into the clinic setting, however, the question of 'dosing' of MGE cell grafts will need to be addressed. Interestingly, it has been reported that an increase in inhibition reaches a plateau with relatively low numbers of transplanted interneurons (Southwell et al., 2010). This suggests that larger numbers of interneurons are unlikely to result in adverse effects, but at the same time, smaller, less intrusive deposits of cells may produce an optimal response. In addition, further evaluation of long-term graft survival and safety should be assessed before undertaking clinical applications. Porcine human simulation neurosurgery is presently underway to establish such criteria prior to human trials (Cunningham et al., unpublished data). In addition, isolation and purification of cortical interneuron populations using appropriate cell surface markers will facilitate the generation of quality-controlled cell sources for human trials. With prudent preclinical testing, this technology holds promise as a therapeutic approach for TLE as well as other intractable diseases of the central nervous system.

Experimental Procedures

PSC culture and differentiation into MGE cells

H7 hESC was maintained and differentiated into MGE cells as described previously (Kim et al., 2014). Differentiated MGE cells were subject to FACS after staining using anti-ENCAM antibody (BD) prior to transplantation. Detailed information can be found in Suppl. Experimental Procedures.

Induction of temporal lobe epilepsy (TLE) in Nod-Scid mice

For induction of TLE, 7-week old male and female Nod-Scid mice (Charles River Laboratory) were injected with 400mg/kg Pilocarpine i.p., 30 minutes after N-methylscopolamine bromide (1 mg/kg, ip) administration to reduce peripheral cholinergic effects (Mazzuferi et al.). To limit the duration of status epilepticus (SE) and extent of damage in the hippocampus, diazepam (10 mg/kg) was injected ip 90 min after seizure induction. The severity of convulsive responses was monitored and classified according to the modified Racine scale (Shibley and Smith, 2002). Ten days after pilocarpine injection, mice that showed stage 3, 4 or 5 seizures were subject to 7 days of continuous video monitoring for spontaneous recurrent seizure (SRS). Mice showing SRS with stage 3, 4 or 5 during the 7-day recording period were designated as "TLE mice" in this study, and they were randomly assigned for subsequent transplantation and behavioral analysis. Detailed information can be found in Suppl. Experimental Procedures.

Transplantation of hMGE cells into hippocampus of TLE model mice

Differentiated and FACS-sorted human MGE cells were transplanted into TLE model mice at the following coordinates: AP −1.75 mm, L ±2.3 mm, V −1.7 mm for the rostral CA3 site; AP −3.25 mm, L ±3.0 mm, V −3.65 mm, −2.9 mm and −2.0 mm for the three caudal sites along the dorso-ventral axis of the hippocampus in this coronal plane. A total of 5×10^4 MGE cells in a 0.5 μl volume were delivered at each of the target coordinates. Sterile, stainless steel bone screw recording electrodes (diameter 0.5mm, length 1.1mm; Plastics One) soldered with a lead wire were placed epidurally through rostral burr holes in the skull (AP −1.75 mm, L ±2.3 mm), and reference electrodes were positioned caudal to lambda.

Electrodes were secured with a rapidcuring dental cement (DenMat Holdings, Lompoc, CA). Detailed information is in Suppl. Experimental Procedures.

Behavioral analysis

Continuous Video-EEG recording of transplanted mice—Three months after transplantation, seizure activity of control or MGE-transplanted TLE mice was recorded using a MP150 Biopac data acquisition System, EEG100C EEG amplifier module and AcqKnowledge 4.0 EEG Acquisition and Reader Software (BIOPAC Systems Inc.) along with Eco Black Box security camera system (Lorex Technology). EEG seizures with high-frequency, high-voltage synchronized polyspike profiles with amplitudes greater than 2-fold that of background and a duration of greater than 15 sec (Hunt et al., 2013) were analyzed using AcqKnowledge 4.0 EEG Acquisition and Reader Software (BIOPAC Systems Inc.) by investigators who were blind to treatment conditions. This was followed by confirmation of EEG seizure activity by video recording.

Y maze—We used a three-arm Y maze for this study: each arm 3 cm wide, 40 cm in length, and with a wall height of 12 cm. Mice were initially placed within one arm, and the sequence and number of entries was recorded for each mouse over a 10 min period.

Novel object recognition test—For a training session, each mouse was placed into an open field box (42 × 42 × 31 cm) containing two identical objects and allowed to freely explore for 3 min. One hour after the training session, one of the familiar objects was replaced with a novel object (defined as the test session). The time that each animal spent exploring the novel object compared to the familiar object was recorded and traced using Ethovision software (Noldus, Wageningen, The Netherlands).

Locomotion test—The home cage (7 1/2” × 11 1/2” × 5”) containing an individual mouse was placed in the center of a photobeam activity system (PAS) monitoring frame (San Diego Instruments) with 4×8 photobeam configuration for 15 min under standard overhead lighting conditions. Total photobeam break numbers were detected by PAS software.

Handling test—Aggressiveness of the mice was assessed as described previously (Hunt et al., 2013) with some modifications. Each of the following three tasks was performed for 15 sec: 1) nonstressful handling (stroking slowly along the back of the mouse in the direction of the grain of fur), 2) stressful handling (vigorous stroking against the grain of the fur), 3) pinching at the tail base with a rubber-ended forceps (Fine Science tools). Reaction to each handling was scored by investigators blinded to treatment conditions using the following rating scale: 1- initial struggle, but calmed within 15 sec, 2- struggle for more than 15 sec, 3- struggle for more than 15 sec and exhibiting one or more defensive reactions (piloerection, flattening of the ears against the head, attempt to bite or back away from the experimenter), and 4- struggled for more than 15 sec and exhibited flight behavior (loud vocalization or wild running). Summation of these three scores provided a total aggressiveness score for each mouse.

More detailed information of behavioral analysis is in Supplemental Experimental Procedures.

Immunohistochemistry, Cell counting and statistical analysis

Transplanted mice were terminally anesthetized with an ip overdose of pentobarbital (150 mg/kg, Sigma) and perfused transcardially with heparin saline (0.1 % heparin in saline) followed by paraformaldehyde (4 %) 2 weeks or 4 months post grafting. Brains were removed, postfixed in 4 % paraformaldehyde for 12 hours, equilibrated in 20 % sucrose/PBS solution, and then sectioned coronally at 40-μm using a freezing microtome. Histological analysis was done as described previously (Kim et al., 2014) and detailed information is in Suppl. Experimental Procedures.

Transmission Electron Microscopy (TEM)

See Supplemental Experimental Procedures for details.

Statistical Analysis

For statistical analysis, we performed a t-test ($\alpha = 0.05$) for comparison of two groups using Prism6 software (Graph Pad). For multiple sample comparison, we performed analysis of variance (ANOVA) with an α level of 0.05 to determine possible statistical differences between group means. When significant differences were found, post hoc analysis was performed using Fisher's LSD ($\alpha = 0.05$) again using Prism6 software. For samples with unequal variances, nonparametric Kruskal-Wallis test was performed using Prism6 software.

Electrophysiology, optogenetic stimulations and Neurolucida tracing

For electrophysiological studies, MGE cells were infected with lentivirus that express ChR2 (H134R)-GFP fusion protein under the control of synapsin promoter (UPenn vector core facility) at day 14 of differentiation. Transduction efficiency was 26.3 ± 4.7 % (n = 4). The cells underwent FACS and were transplanted as described above. Two to five months after transplantation, acute brain slices containing the hippocampus were prepared using a vibrating microtome for electrophysiological analysis. After recovery, brain slices were placed in the recording chamber and continuously perfused at the rate of 1 mL per minute with the artificial cerebrospinal fluid containing 130 mM NaCl, 2.5 mM KCl, 2.5 mM $CaCl_2$, 1 mM $MgSO_4$, 1.25 mM NaH_2PO_4, 26 mM $NaHCO_3$, and 10 mM glucose with 95 % O_2 and 5 % CO_2. Whole-cell patch-clamp recordings were performed at 31–33°C using EPC-9 amplifier and Pulse v8.8 software (HEKA Elektronik). For recording grafted MGE-derived neurons (GFP^+ cells) and host hippocampal interneurons, the patch electrodes (~5 MOhm resistance) were filled with solution containing 150 mM K-gluconate, 5 mM NaCl, 1 mM $MgCl_2$, 10 mM HEPES, 0.2 EGTA, 2 mM MgATP, 0.5 mM NaGTP, and 5 mM biocytin (290 mOsm, adjusted to pH 7.3 with KOH). For recording GFP^- host hippocampal neurons, the patch electrodes were filled with solution containing 140 mM Cs-methanesulfonate, 5 mM NaCl, 1 mM $MgCl_2$, 10 mM HEPES, 0.2 EGTA, 2 mM MgATP, 0.5 mM NaGTP, 5 mM QX 314 chloride, and 5 mM biocytin (290 mOsm, adjusted to pH 7.3 with CsOH). Liquid junction potential of 15.5 and 8.9 mV was corrected for the K-gluconate-based and Cs-based pipette solutions, respectively. Series (access) resistance was not compensated. Blue collimated light-emitting diode (LED) with 470 nm peak wavelength (M470L2, Thorlabs) was used for photostimulations of grafted MGE-derived cells expressing ChR2-GFP. Brain slices in the recording chamber were illuminated through a

40× water-immersion objective lens (IR-Achroplan, Carl Zeiss). Illumination area was 0.26 mm^2 and was centered at the cell patched for recording.

Offline data analysis was performed using Clampfit 9 program (Molecular Devices). Reagents were purchased from Tocris Bioscience (QX 314 chloride, biocytin, and NBQX) or Sigma-Aldrich (ATP, GTP, and bicuculline methochloride). For statistical analyses of electrophysiological data, we used ANOVA with Bonferroni's simultaneous multiple comparisons. Statistical analysis was performed with Minitab16 software (Minitab) and $p < 0.05$ was considered statistically significant.

After electrophysiological recordings, brain slices were fixed in 4 % paraformaldehyde at 4°C overnight. Recorded cells loaded with biocytin were labeled with streptavidin, Alexa 568 conjugate (20 μg/mL in PBS, Molecular Probes) as described previously (Cho et al., 2013). Images of biocytin/streptavidin-labelled cells were taken with z-stack function using Leica TSC SP8 confocal microscope. The confocal images were then used for neuron tracing with Neurolucida software (Microbright Field, Williston, VT).

Single cell reverse transcription-polymerase chain reaction (scRT-PCR)

See Supplementary Experimental Procedures for details.

Supplementary Material

Refer to Web version on PubMed Central for supplementary material.

Acknowledgements

This study was supported by NIH grants (NS079977), NIH grant (NS070577), NIH grant (MH090464) and Harvard Stem Cell Institute Seed Grant. We thank Drs. Uwe Rudolph, Christopher Cowan and Joseph Coyle for sharing animal behavioral equipment. We thank Dr. Pachnis for kind gift of anti-Lhx6 antibodies and Dr. Palmiter for anti-ZnT3 antibodies.

KK, VB and SC supported this study financially.

References

Baraban SC, Southwell DG, Estrada RC, Jones DL, Sebe JY, Alfaro-Cervello C, Garcia-Verdugo JM, Rubenstein JL, Alvarez-Buylla A. Reduction of seizures by transplantation of cortical GABAergic interneuron precursors into Kv1.1 mutant mice. Proc Natl Acad Sci U S A. 2009; 106:15472–15477. [PubMed: 19706400]

Bjarkam CR, Glud AN, Margolin L, Reinhart K, Franklin R, Deding D, Ettrup KS, Fitting LM, Nielsen MS, Sorensen JC, et al. Safety and function of a new clinical intracerebral microinjection instrument for stem cells and therapeutics examined in the Gottingen minipig. Stereotactic and functional neurosurgery. 2010; 88:56–63. [PubMed: 20051711]

Brooks-Kayal AR, Bath KG, Berg AT, Galanopoulou AS, Holmes GL, Jensen FE, Kanner AM, O'Brien TJ, Whittemore VH, Winawer MR, et al. Issues related to symptomatic and disease-modifying treatments affecting cognitive and neuropsychiatric comorbidities of epilepsy. Epilepsia. 2013; 54(Suppl 4):44–60. [PubMed: 23909853]

Chen KG, Mallon BS, McKay RD, Robey PG. Human pluripotent stem cell culture: considerations for maintenance, expansion, and therapeutics. Cell Stem Cell. 2014; 14:13–26. [PubMed: 24388173]

Cho JH, Deisseroth K, Bolshakov VY. Synaptic encoding of fear extinction in mPFC-amygdala circuits. Neuron. 2013; 80:1491–1507. [PubMed: 24290204]

Christoph CH. Temporal lobe resection--does the prospect of seizure freedom outweigh the cognitive risks? Nat Clin Pract Neurol. 2008; 4:66–67. [PubMed: 17955042]

Cossart R, Dinocourt C, Hirsch JC, Merchan-Perez A, De Felipe J, Ben-Ari Y, Esclapez M, Bernard C. Dendritic but not somatic GABAergic inhibition is decreased in experimental epilepsy. Nature neuroscience. 2001; 4:52–62.

Cramer JA, Mintzer S, Wheless J, Mattson RH. Adverse effects of antiepileptic drugs: a brief overview of important issues. Expert Rev Neurother. 2010; 10:885–891. [PubMed: 20518605]

Curia G, Longo D, Biagini G, Jones RS, Avoli M. The pilocarpine model of temporal lobe epilepsy. J Neurosci Methods. 2008; 172:143–157. [PubMed: 18550176]

de Lanerolle NC, Kim JH, Robbins RJ, Spencer DD. Hippocampal interneuron loss and plasticity in human temporal lobe epilepsy. Brain Res. 1989; 495:387–395. [PubMed: 2569920]

Doischer D, Hosp JA, Yanagawa Y, Obata K, Jonas P, Vida I, Bartos M. Postnatal differentiation of basket cells from slow to fast signaling devices. J Neurosci. 2008; 28:12956–12968. [PubMed: 19036989]

Engel J. A Proposed Diagnostic Scheme for People with Epileptic Seizures and with Epilepsy: Report of the ILAE Task Force on Classification and Terminology. Epilepsia. 2001; 42:796–803. [PubMed: 11422340]

Engel J. Epilepsy in the world today: medical point of view. Epilepsia. 2002; 436(Suppl 6):12–13. [PubMed: 12190969]

Fine A, Meldrum BS, Patel S. Modulation of experimentally induced epilepsy by intracerebral grafts of fetal GABAergic neurons. Neuropsychologia. 1990; 28:627–634. [PubMed: 2168529]

Groticke I, Hoffmann K, Loscher W. Behavioral alterations in the pilocarpine model of temporal lobe epilepsy in mice. Exp Neurol. 2007; 207:329–349. [PubMed: 17714705]

Hattiangady B, Rao MS, Shetty AK. Grafting of striatal precursor cells into hippocampus shortly after status epilepticus restrains chronic temporal lobe epilepsy. Exp Neurol. 2008; 212:468–481. [PubMed: 18579133]

Hirsch JC, Agassandian C, Merchan-Perez A, Ben-Ari Y, DeFelipe J, Esclapez M, Bernard C. Deficit of quantal release of GABA in experimental models of temporal lobe epilepsy. Nature neuroscience. 1999; 2:499–500.

Hunt RF, Girskis KM, Rubenstein JL, Alvarez-Buylla A, Baraban SC. GABA progenitors grafted into the adult epileptic brain control seizures and abnormal behavior. Nature neuroscience. 2013; 16:692–697.

Jensen FE. Epilepsy in 2013: Progress across the spectrum of epilepsy research. Nat Rev Neurol. 2014; 10:63–64. [PubMed: 24419682]

Kim T-G, Yao R, Monnell T, Cho J-H, Vasudevan A, Koh A, Peeyush KT, Moon M, Datta D, Bolshakov VY, et al. Efficient Specification of Interneurons from Human Pluripotent Stem Cells by Dorsoventral and Rostrocaudal Modulation. STEM CELLS. 2014; 32:1789–1804. [PubMed: 24648391]

Kobayashi M, Buckmaster PS. Reduced inhibition of dentate granule cells in a model of temporal lobe epilepsy. J Neurosci. 2003; 23:2440–2452. [PubMed: 12657704]

Le Magueresse C, Monyer H. GABAergic Interneurons Shape the Functional Maturation of the Cortex. Neuron. 2013; 77:388–405. [PubMed: 23395369]

Lindvall O, Bjorklund A. Intracerebral grafting of inhibitory neurons. A new strategy for seizure suppression in the central nervous system. Advances in neurology. 1992; 57:561–569. [PubMed: 1543081]

Loscher W, Ebert U, Lehmann H, Rosenthal C, Nikkhah G. Seizure suppression in kindling epilepsy by grafts of fetal GABAergic neurons in rat substantia nigra. J Neurosci Res. 1998; 51:196–209. [PubMed: 9469573]

Maisano X, Litvina E, Tagliatela S, Aaron GB, Grabel LB, Naegele JR. Differentiation and functional incorporation of embryonic stem cell-derived GABAergic interneurons in the dentate gyrus of mice with temporal lobe epilepsy. J Neurosci. 2012; 32:46–61. [PubMed: 22219269]

Mallon BS, Chenoweth JG, Johnson KR, Hamilton RS, Tesar PJ, Yavatkar AS, Tyson LJ, Park K, Chen KG, Fann YC, et al. StemCellDB: the human pluripotent stem cell database at the National Institutes of Health. Stem cell research. 2013; 10:57–66. [PubMed: 23117585]

Marco P, Sola RG, Pulido P, Alijarde MT, Sanchez A, Ramon y Cajal S, DeFelipe J. Inhibitory neurons in the human epileptogenic temporal neocortex. An immunocytochemical study. Brain. 1996; 119(Pt 4):1327–1347. [PubMed: 8813295]

Mazzuferi M, Kumar G, Rospo C, Kaminski RM. Rapid epileptogenesis in the mouse pilocarpine model: video-EEG, pharmacokinetic and histopathological characterization. Exp Neurol. 2012; 238:156–167. [PubMed: 22960187]

Muller CJ, Groticke I, Bankstahl M, Loscher W. Behavioral and cognitive alterations, spontaneous seizures, and neuropathology developing after a pilocarpine-induced status epilepticus in C57BL/6 mice. Exp Neurol. 2009; 219:284–297. [PubMed: 19500573]

Nicholas CR, Chen J, Tang Y, Southwell DG, Chalmers N, Vogt D, Arnold CM, Chen YJ, Stanley EG, Elefanty AG, et al. Functional Maturation of hPSC-Derived Forebrain Interneurons Requires an Extended Timeline and Mimics Human Neural Development. Cell Stem Cell. 2013; 12:573–586. [PubMed: 23642366]

Okaty BW, Miller MN, Sugino K, Hempel CM, Nelson SB. Transcriptional and electrophysiological maturation of neocortical fast-spiking GABAergic interneurons. J Neurosci. 2009; 29:7040–7052. [PubMed: 19474331]

Rice AC, Floyd CL, Lyeth BG, Hamm RJ, DeLorenzo RJ. Status epilepticus causes long-term NMDA receptor-dependent behavioral changes and cognitive deficits. Epilepsia. 1998; 39:1148–1157. [PubMed: 9821978]

Shibley H, Smith BN. Pilocarpine-induced status epilepticus results in mossy fiber sprouting and spontaneous seizures in C57BL/6 and CD-1 mice. Epilepsy Res. 2002; 49:109–120. [PubMed: 12049799]

Southwell, DG.; Froemke, RC.; Alvarez-Buylla, A.; Stryker, MP.; Gandhi, SP. Science. Vol. 327. New York, NY: 2010. Cortical plasticity induced by inhibitory neuron transplantation; p. 1145-1148.

Southwell, DG.; Nicholas, CR.; Basbaum, AI.; Stryker, MP.; Kriegstein, AR.; Rubenstein, JL.; Alvarez-Buylla, A. Science. Vol. 344. New York, NY: 2014. Interneurons from embryonic development to cell-based therapy; p. 1240622

Spreafico R, Battaglia G, Arcelli P, Andermann F, Dubeau F, Palmini A, Olivier A, Villemure JG, Tampieri D, Avanzini G, et al. Cortical dysplasia: an immunocytochemical study of three patients. Neurology. 1998; 50:27–36. [PubMed: 9443453]

Walia KS, Khan EA, Ko DH, Raza SS, Khan YN. Side effects of antiepileptics--a review. Pain practice : the official journal of World Institute of Pain. 2004; 4:194–203. [PubMed: 17173601]

Wieser HG. ILAE Commission Report. Mesial temporal lobe epilepsy with hippocampal sclerosis. Epilepsia. 2004; 45:695. [PubMed: 15144438]

Yu DX, Marchetto MC, Gage FH. Therapeutic translation of iPSCs for treating neurological disease. Cell Stem Cell. 2013; 12:678–688. [PubMed: 23746977]

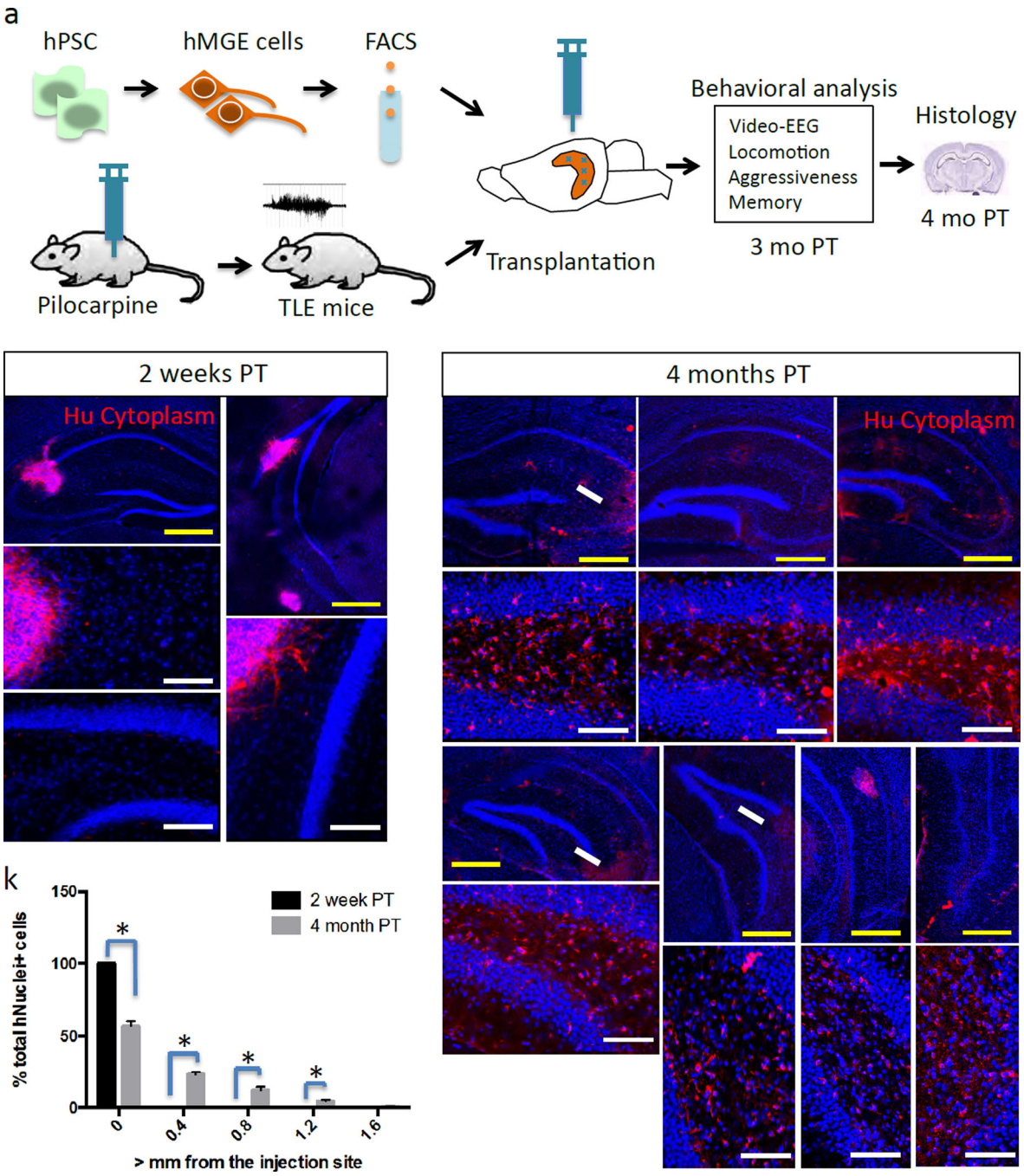

Figure 1. Transplanted human mGIN migrate robustly and integrate in adult epileptic brains (See also Figure S1–S4)

(a) Overall experimental design. hPSC-derived MGE cells were transplanted into the hippocampus of TLE mice. Behavioral analysis was conducted after 3 months PT and histology analysis at 4 months PT. (b–c) Two weeks PT, transplanted cells display minimal migration, shown by human cytoplasm-specific antibody staining (b', b", c' show enlarged photomicrographs of dentate gyrus regions from corresponding pictures). (d–j) Four month PT, transplanted cells display robust migration and integration into the host brain, as shown by human cytoplasm-specific antibodies (d'–j' show enlarged photomicrographs of dentate

gyrus regions from corresponding pictures, depicting migration from the injection site). White arrows indicate injection sites. Yellow scale bars: 500 μm. White scale bars: 100 μm. (k) Quantification of migration of transplanted cells (Mean ± S.E.M.; *P<0.05, two tailed t-test) 2 week PT (n=3) and 4 month PT (n=8).

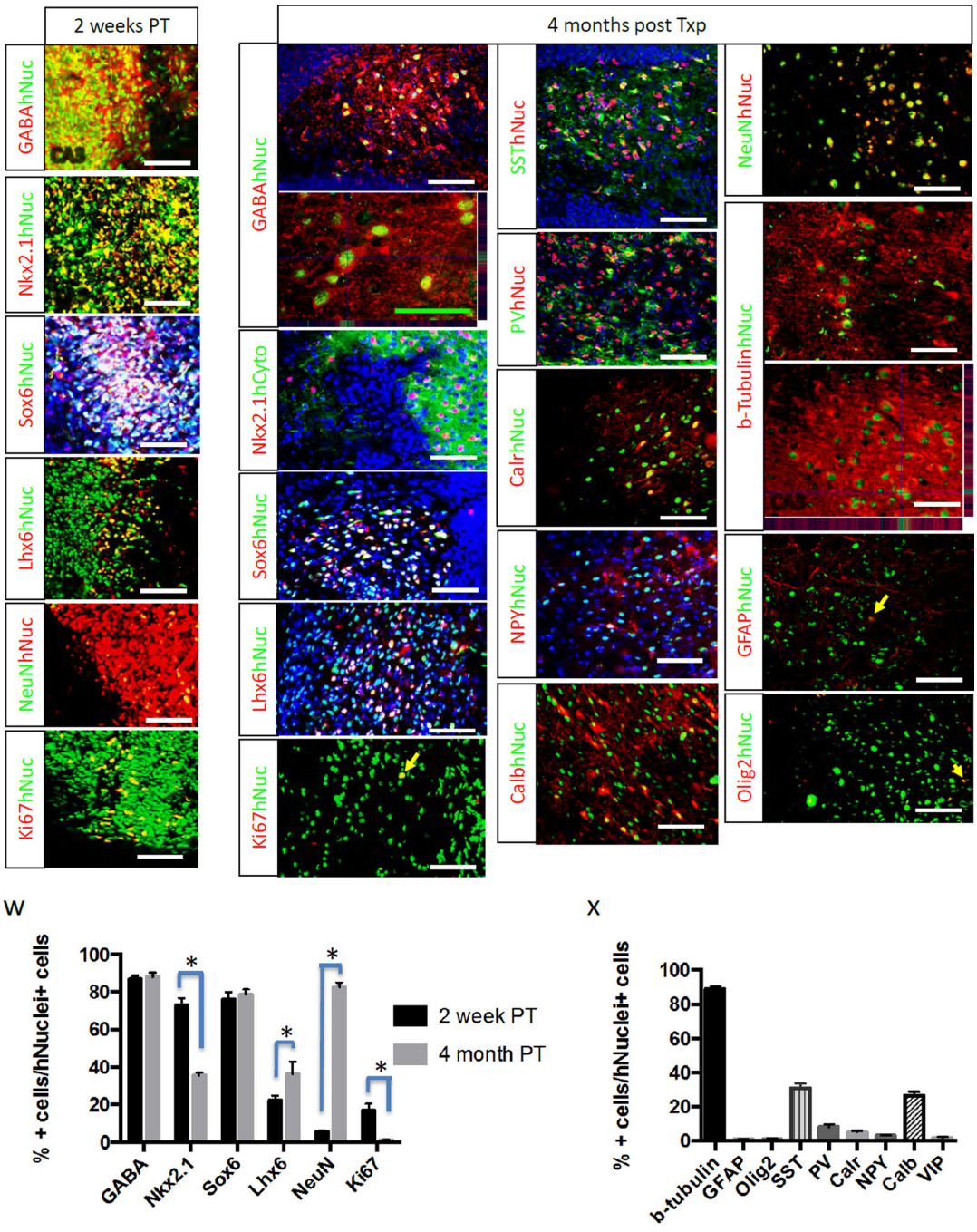

Figure 2. Transplanted human MGE cells generate mGIN in adult epileptic brains (See also Figure S5)

(a–f) Immunohistochemical analysis of transplanted cells 2 weeks PT. (g–v) Immunohistochemical analysis of transplanted cells 4 months PT. SST, somatostatin; PV, parvalbumin; Calr, calreticulin; NPY, neuropeptide Y; Calb, calbindin. Green scale bar: 50 μm. White scale bars: 100 μm. (w) Cell counting analysis of 2 weeks PT vs. 4 months PT (Mean ±S.E.M.; n=3, *P<0.05, two tailed t-test). (x) Cell counting analysis at 4 months PT (n=3).

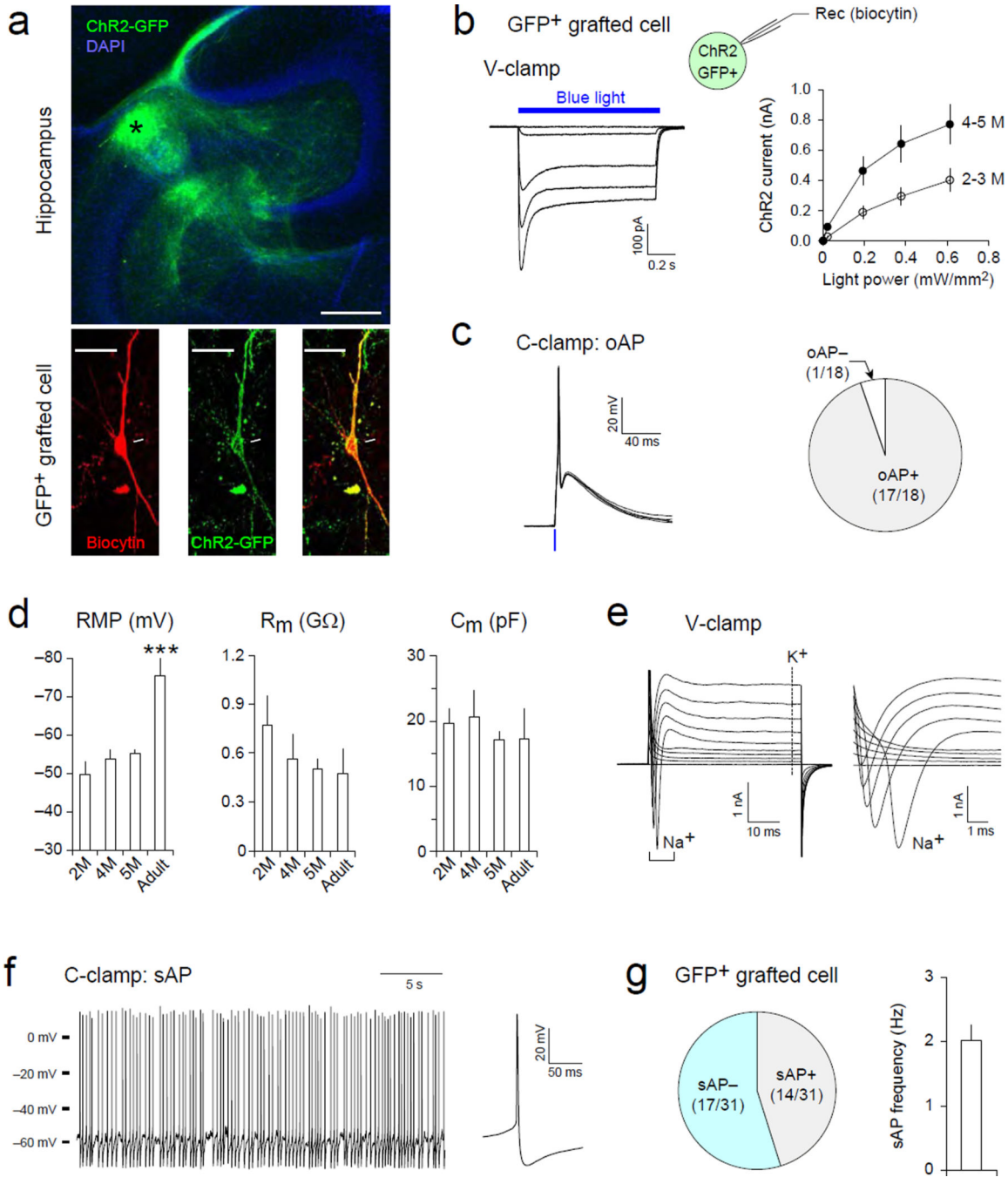

Figure 3. Electrophysiological characterization of grafted human mGIN in the hippocampus

(a) Top, a microscopic image showing the distribution of grafted human mGIN in the hippocampus. Channelrhodopsin 2 (ChR2)/GFP -expressing human MGE cells (green) transplanted into the cornu ammonis region 3 (CA3) of the hippocampus, migrate extensively to the CA1 and dentate gyrus (DG). The graft core is indicated by an asterisk. Strata oriens (s.o.), pyramidale (s.p.), and radiatum (s.r.) are also indicated. Bottom, confocal microscopic images showing that the recorded grafted cell, labeled with biocytin-streptavidin (red, left panel), expresses ChR2-GFP (green, middle panel). **(b)** Whole-cell

patch-clamp recordings were performed with grafted cells expressing ChR2-GFP. Grafted human mGIN were identified with green fluorescence in acute brain slices. Biocytin was included in the pipette solution to label the recorded cells. Left, representative traces of ChR2-mediated currents in a grafted cell. These inward currents were induced by blue light illuminations (470 nm, 1 s pulses, blue horizontal bar) with variable intensities (0.02–0.61 mW/mm^2) and recorded at –80 mV in voltage-clamp mode (V-clamp). Right, a summary graph showing the peak amplitude of ChR2-mediated currents plotted versus light power. ChR2 currents were larger in human mGIN 4–5 months after transplantation (n = 16 cells) than in cells 2–3 months after implantation (n = 9 cells) ($p < 0.001$). **(c)** Representative traces of action potentials (AP) evoked by short pulses of blue light illumination (1 ms, 12.5 mW/mm^2, blue vertical line, left panel). These optogenetically-induced APs (oAP) were recorded in current-clamp mode (C-clamp) at approximate –85 mV and were detected in most grafted human mGIN examined (n = 18 cells, right panel). **(d)** Summary plots of resting membrane potential (RMP), membrane resistance (R_m), and a fast component of membrane capacitance (C_m) of grafted human mGIN, which were examined 2, 4, or 5 months after transplantation (n = 6, 8, and 11 cells, respectively), as well as host adult hippocampal interneurons (Adult, > 3 months old, n = 4 cells). *** $p < 0.001$, adult versus all other groups. **(e)** Representative traces showing currents induced by voltage pulses in a grafted cells. Membrane potential was held at –85 mV in voltage-clamp mode. Left, square voltage pulses from –85 mV to 5 mV with increment of 10 mV (50 ms long) induced both transient inward (Na^+, a bracket) and sustained outward currents (K^+, a vertical dotted line), which are likely to be mediated by voltage-gated Na^+ and K^+ channels, respectively. Right, the same trace was zoomed in to visualize the transient inward currents mediated by voltage-gated Na^+ channels. **(f)** A representative trace of spontaneous AP firings (sAP) in a grafted human mGIN. AP firings were recorded at RMP in current-clamp mode without current injection or withdrawal. A trace on the right is the average of sAP recorded in the same neuron. (**g**) Left, spontaneous APs (sAP) were detected at RMP in 45 % of total 31 grafted cells examined. Right, a summary graph showing the average frequency of sAP (n = 14 cells). Error bars are SEM.

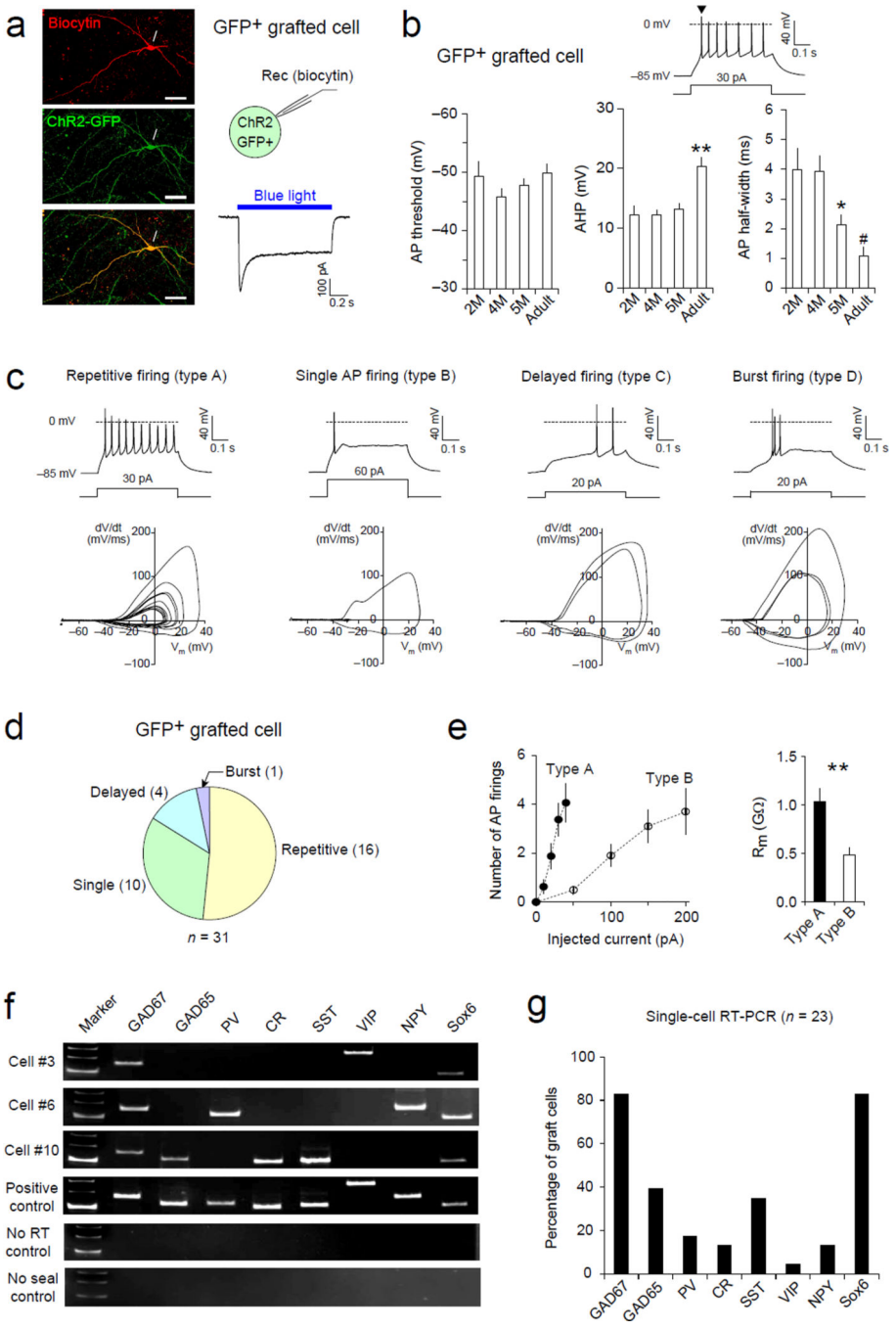

Figure 4. Transplanted human MGE cells differentiate into GABAergic interneurons in the epileptic hippocampus (See also Figure S6)

(a) Left, microscopic images of a recorded human MGE cell in acute hippocampal slices. ChR2/GFP-expressing human MGE cells were identified with green fluorescence and labeled with biocytin-streptavidin (red) using recording pipettes. Right, blue light illumination (470 nm, 0.61 mW/mm^2, blue horizontal bar) induces ChR2-mediated currents recorded at –80 mV in voltage-clamp mode, confirming that the recorded cell is a grafted cell. **(b)** Analysis of action potential (AP) firings in human mGIN transplanted into the

hippocampus. Top, a representative trace of AP firings in a ChR2/GFP-expressing grafted cell. APs were induced by depolarizing current injection near threshold (500 ms long) and recorded in current-clamp mode at approximate –85 mV. The amount of injected currents is indicated below the trace. For each grafted cell, the first AP (an arrowhead) was analyzed. Bottom, summary graphs showing the average AP threshold (left), afterhyperpolarization (AHP, middle), and AP half-width (right) in human mGIN examined 2, 4, and 5 months after transplantation (n = 6, 8, and 11 cells, respectively) as well as host adult hippocampal interneurons. (Adult, > 3 month old, n = 4 cells). ** $p < 0.01$, adult versus all other groups; * $p < 0.05$, 5 month versus 4 month group; # $p < 0.05$, adult versus 2 or 4 month group. Error bars are SEM. **(c)** Representative traces (top row) and phase plots (bottom row) of four different types of AP firings recorded in grafted human mGIN in hippocampal slices. APs were induced by near-threshold depolarizing current injections in GFP^+ grafted cells and were recorded as in (b). Most grafted cells displayed either repetitive firings (type A, first column) or single AP firing (type B, second column) while delayed (type C, third column) or burst firing patterns (type D, fourth column) were observed in a small proportion of grafted cells. Repetitive AP firings could be induced by small current injections in type A cells (< 50 pA) whereas type B cells fires only a few APs, which required relatively larger current injections (> 50 pA). The amount of injected currents is indicated below the traces. Baseline membrane potential was approximately –85 mV. **(d)** A summary graph showing the proportion of grafted human MGE-derived cells displaying four different AP firing patterns (n = 31 cells). **(e)** Left, a summary plot of AP firings in human mGIN in the hippocampus. The number of AP firings was plotted versus injected currents (500 ms long). Note more frequent AP firings induced by small current injections in type A cells (n = 16 cells) than in type B cells (n = 10 cells). Right, the average membrane resistance (R_m) in type A was larger significantly than in type B cells. ** $p < 0.01$. Error bars are SEM. **(f)** Examples of RNA profiles of three grafted cells from single-cell RT-PCR (scRT-PCR, top three rows). Intracellular contents of grafted cells were harvested individually after whole-cell patch-clamp recordings. Positive control with total RNA from the human brain as well as two negative controls (no RT control and no giga-seal formation) are also included in middle and bottom rows. M, size marker (300, 200 and100 bp from top to bottom); PV, parvalbumin; CR, calreticulin; SST, somatostatin; VIP, vasoactive intestinal peptide; NPY, neuropeptide Y. **(g)** A summary plot of RNA profile of grafted human mGIN from scRT-PCR (n = 23 cells).

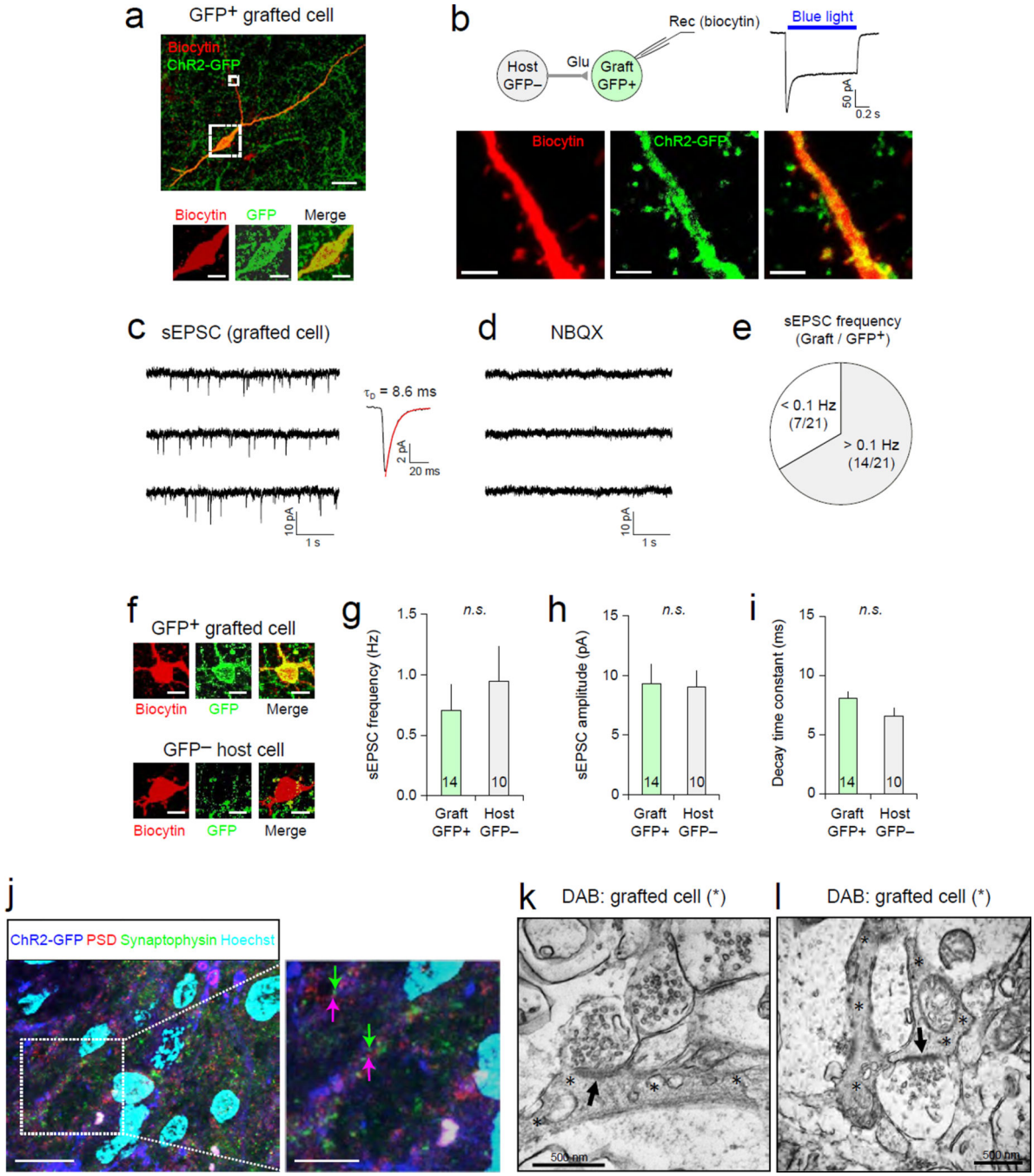

Figure 5. Transplanted human mGIN receive glutamatergic inputs from host neurons

(a) A representative image of a human mGIN transplanted into the hippocampus (green). The ChR2/GFP-expressing grafted cell was labeled with biocytin using a recording patch pipette (red). The cell body is indicated as a larger dotted square and is zoomed in below the image. **(b)** Top left, grafted human mGIN were recorded in acute brain slices. Grafted cells, identified with green fluorescence, receive synaptic inputs from host neurons. The recorded cell was labeled with biocytin-streptavidin (red) using patch pipettes. Top right, blue light illumination induced inward currents, confirming that the recorded cell is a grafted cell

expressing ChR2-GFP. ChR2- mediated currents were induced and recorded as in Figure 4(a). Bottom, confocal microscopic images show a portion of dendrites of the recorded human mGIN and are the zoomed-in images of that indicated as a smaller dotted square in (a). Dendritic spines are indicated by asterisks. **(c)** Left, a representative trace of postsynaptic responses recorded in a GFP^+ grafted cell. Spontaneous excitatory postsynaptic currents (sEPSCs) were recorded in GFP^+ grafted cells at − 85 mV in voltage-clamp mode. Right, a trace showing the average of sEPSCs recorded in the same cell. Decay time constant (τ_D) of sEPSC was calculated by fitting the decay phase of the trace to a single exponential function (red curve). **(d)** The application of 10 μM NBQX inhibited sEPSC completely in the same grafted cell as in (c), indicating that sEPSCs were mediated by AMPA/kainate-type glutamate receptors and that the grafted cell receives functional synaptic inputs from host glutamatergic neurons. n = 4 cells. **(e)** Two thirds of recorded human mGIN displayed spontaneous postsynaptic responses with the frequency > 0.1 Hz. **(f)** Representative images of the cell bodies of GFP^+ grafted cells (top) and GFP^- host hippocampal interneurons (bottom). The recorded cells were labeled with biocytin-streptavidin (red) as in (a). **(g–i)** Summary plots of the frequency (g), peak amplitude (h), and decay time constant (i) of sEPSC recorded in GFP^+ grafted cells (n = 14) and GFP^- host hippocampal interneurons (n = 10). No significant difference was detected between grafted and host cells (n.s.). Error bars are SEM. **(j)** A representative image of immunohistochemistry analysis of human mGIN transplanted in the hippocampus. Hoechst (sky blue) was used as nuclear counter-stain. Arrows in magenta indicate postsynaptic densities of GFP^+ grafted cells (double-stained with ChR2-GFP and PSD), and green arrows indicate presynaptic axon terminals (stained with synaptophysin, green) of GFPcells. **(k–l)** TEM images showing that grafted human mGIN receive synaptic inputs from host cells. Transplanted cells, stained with DAB for human cytoplasm-specific antibodies (gray areas marked by asterisks), display prominent postsynaptic densities (arrows), receiving presynaptic inputs from DAB^- host cells (no stain).

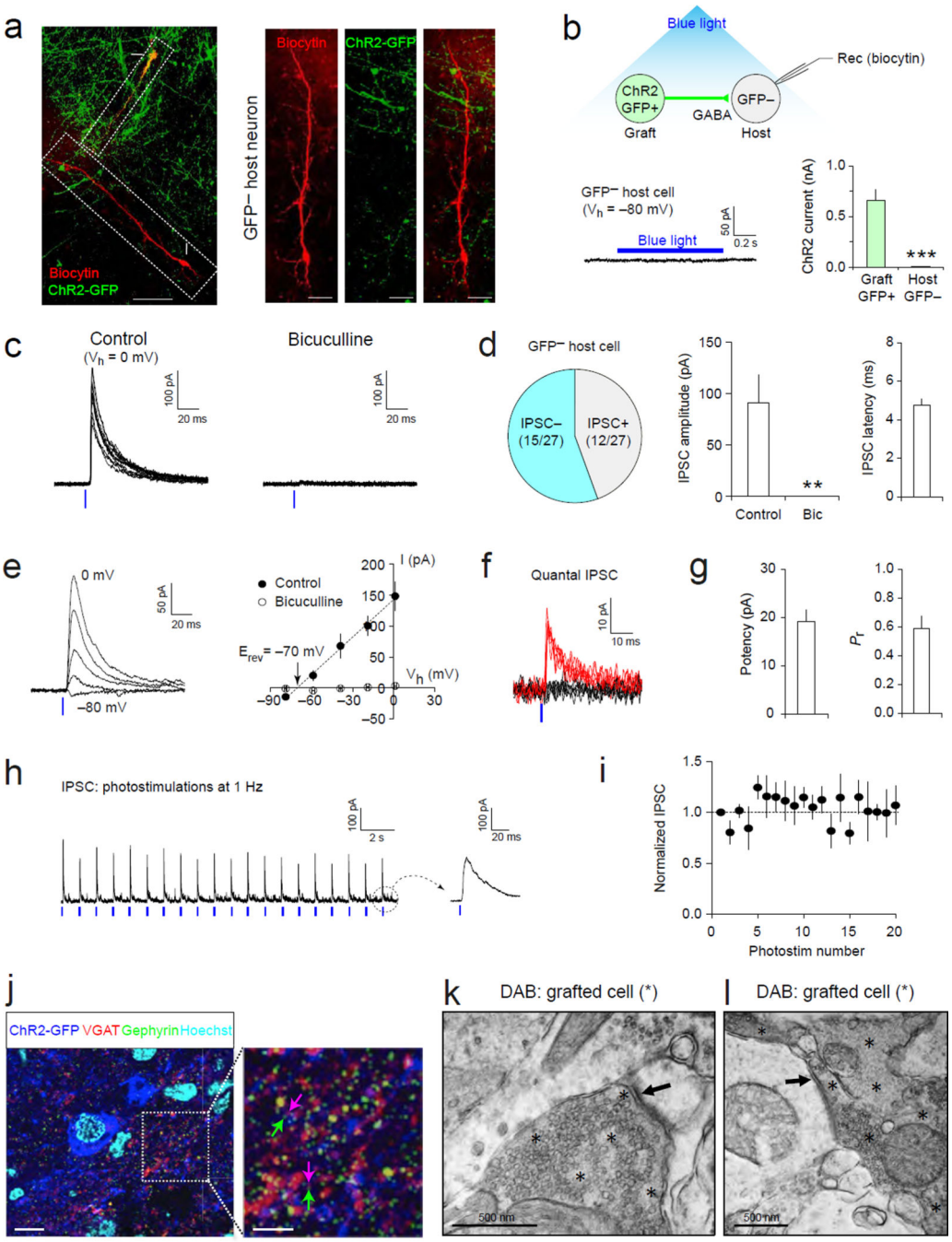

Figure 6. Optogenetic stimulations of transplanted human mGIN induce GABAergic postsynaptic responses in host hippocampal neurons

(a) Left, a microscopic image showing both a GFP$^+$ grafted human MGE cell and a GFP$^-$ host pyramidal neuron in the CA3 of the hippocampus (dotted squares; cell bodies are indicated by arrows). These cells were labeled with biocytin-Streptavidin using recording pipettes (red). The grafted cell sends out projections towards the host pyramidal neuron. Right, microscopic images showing the soma and dendrites of the same GFP$^-$ pyramidal neuron as in the left image. Projections from grafted human mGIN are shown in the middle

panel (green, ChR2-GFP). **(b)** Top, blue light illumination evokes AP firings in GFP^+ mGIN expressing ChR2 and induces the release of GABA at axon terminals, generating postsynaptic responses in the recorded GFP^- host neuron. Bottom left, blue light illumination (0.61 mW/mm^2, blue horizontal bar) did not induce ChR2-mediated current in GFP^- host neurons at −80 mV in voltage-clamp mode, indicating the lack of ChR2 expression. Bicuculline (30 μM) was added to inhibit GABAergic responses in the recorded host neuron. Bottom right, the comparison of ChR2-currents between grafted and host cells (n = 25 and 27 cells, respectively), which received the same blue light illumination (0.61 mW/mm^2). *** $p < 0.001$. **(c)** Left, representative traces of postsynaptic currents recorded in a GFP^- host neuron. Postsynaptic responses were recorded at 0 mV in voltage-clamp mode and induced by photostimulations at 12.5 mW/mm^2 (1 ms duration, blue vertical line). Blue light illumination was applied every 10 seconds. Right, these postsynaptic currents were completely inhibited by the application of $GABA_A$ receptor antagonist, bicuculline (30 μM) in the same neuron. **(d)** Left, 44 % of total 27 GFP^- host neurons displayed $GABA_A$ receptor-mediated inhibitory postsynaptic currents (IPSC) induced by photostimulations. Middle, a summary graph showing the average amplitude of IPSCs before and after the application of bicuculline as in (c). ** $p < 0.01$. Right, a plot showing the average synaptic latency of IPSCs induced optogenetically and recorded in GFP^- host neurons (n = 10 neurons). The synaptic latency was quantified as the time interval between the start of photostimulations and the onset of synaptic responses. **(e)** Left, representative traces of postsynaptic currents recorded in a GFP^- host neuron. Postsynaptic currents were induced by blue light illuminations at 12.5 mW/mm^2 (1 ms duration, blue vertical line) and recorded in voltage-clamp mode at –80, −60, −40, −20, and 0 mV. Right, a current-voltage plot of the postsynaptic responses. Peak amplitudes of postsynaptic currents were plotted versus holding potential (V_h, closed circles). Linear regression (a dotted line) reveals the reversal potential of the postsynaptic currents (E_{rev} = −70 mV). The application of 30 μM bicuculline inhibited postsynaptic currents completely at all holding potentials examined (open circles). n = 3 neurons. **(f)** Overlaid traces of quantal IPSCs (qIPSC) indicate both successes (red traces) and failures (black traces). qIPSCs were induced by blue light illuminations (blue vertical line) and recorded in GFP^- host neurons as in (c). **(g)** Summary plots showing the average potency (quantal size) and release probability (P_r) of qIPSCs. n = 6 neurons. **(h)** A representative trace of IPSCs induced by train photostimulations. IPSCs were induced by blue light illumination applied at 1 Hz (12.5 mW/mm^2, 1 ms duration, blue vertical lines) and recorded in GFP^- host neurons at 0 mV in voltage-clamp mode. A trace on the right indicates the last evoked IPSC (a dotted circle). **(i)** A summary plot of IPSCs during 1 Hz train photostimulations as in (h). The peak amplitude of IPSCs was normalized to the first IPSC (a dotted line; n = 3). **(j)** Immunohistochemistry analysis of transplanted human mGIN. Hoechst (sky blue) was used as nuclear counter-stain. Arrows in magenta indicate GABAergic presynaptic terminals of GFP^+ grafted cells (double-stained with ChR2-GFP and VGAT) and green arrows indicate inhibitory postsynaptic densities (stained with gephyrin, green) of GFPcells. **(k–l)** TEM images of grafted cells stained with DAB for human cytoplasm-specific antibodies (gray areas marked by asterisks). DAB^- host cells (no stain) receives synaptic inputs (arrows) from DAB^+ grafted cells. Error bars are SEM.

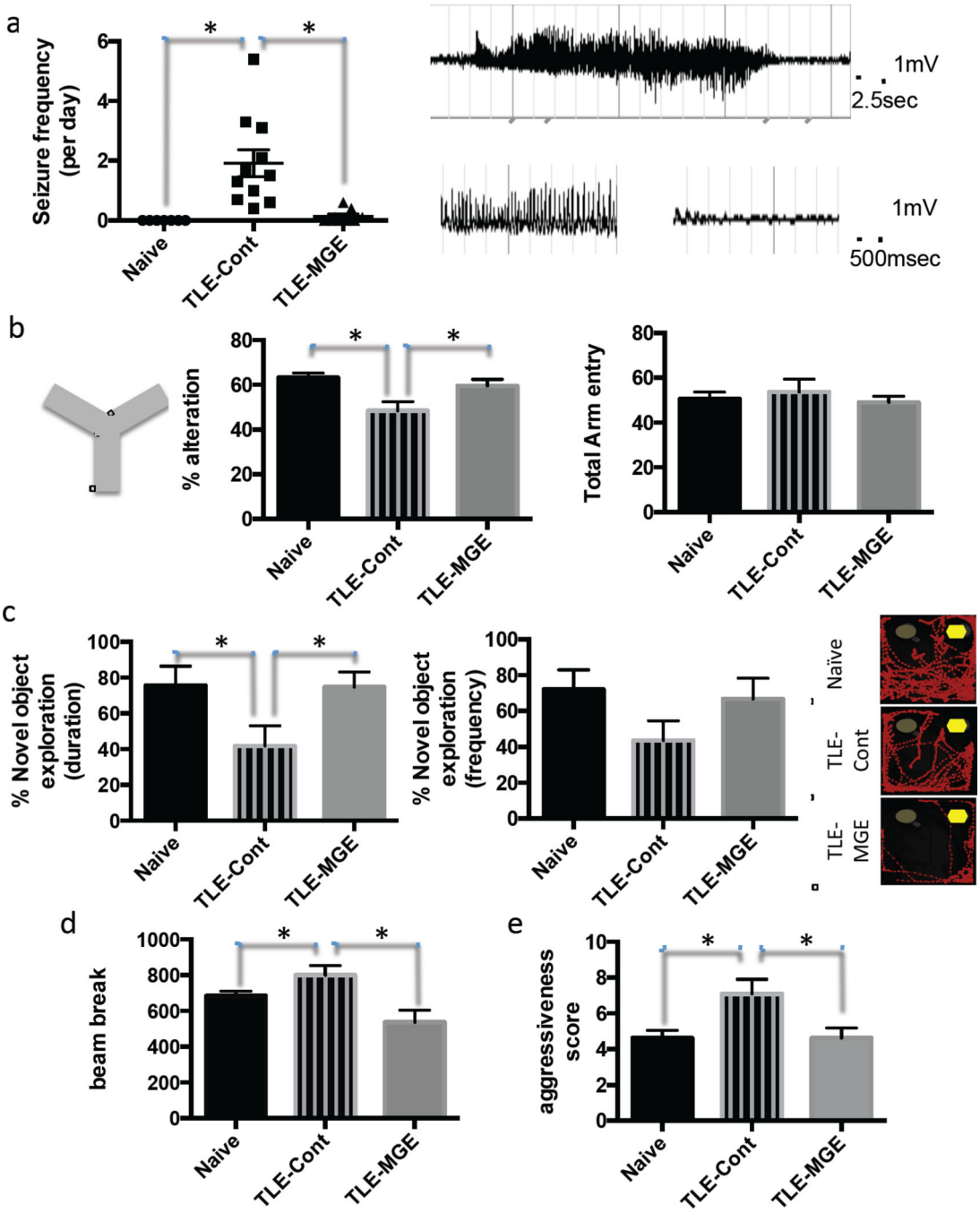

Figure 7. Transplanted mGIN reduce seizure activity and other behavioral abnormalities (See also Figure S7)

(a) Video-EEG analysis of naïve mice (n=6), vehicle-injected control TLE mice (n=11) and MGE-transplanted TLE mice (n=9). Right panel shows representative seizure EEG activity with high-frequency, high-voltage synchronized polyspikes. (b) Y maze test of naïve mice (n=9), vehicle-injected TLE control mice (n=10) and transplanted TLE (n=8), shown by % alternation as an indicative of short-term memory and by the number of total arm entry as an indicative of locomotor activity. (c) Novel object recognition test of naïve mice (n= 12), vehicle-injected TLE control mice (n=11) and transplanted TLE mice (n=8), shown by %

time spent near a novel object to total time spent exploring either object, and by % number of visits near novel object to total number of visits exploring objects. Right panel shows representative tracing of mouse center point during trial, detected using Ethovision software. Novel object is shown as a yellow hexagonal symbol. (d) Locomotion test of naïve mice (n=14), vehicleinjected control TLE mice (n=11) and MGE-transplanted TLE mice (n = 8), shown by the number of photobeam breaks in 15 min. (e) Handling test of naïve mice (n=15), vehicle-injected TLE control mice (n=11) and transplanted TLE mice (n=10). Data are presented as the average ± S.E.M. * $p < 0.05$, ANOVA followed by post hoc analysis using non-parametric Kruskal-Wallis test in (a) and by post hoc analysis using Fisher's LSD in (b)–(e).